

UNIVERSALITY IN HALTING TIME AND ITS APPLICATIONS IN OPTIMIZATION

Levent Sagun, Thomas Trogdon & Yann LeCun

Courant Institute of Mathematical Sciences

New York University

New York, NY 10012, USA

{sagun,trogdon}@cims.nyu.edu, yann@cs.nyu.edu

ABSTRACT

The authors present empirically universal distributions for the halting time (measured by the number of iterations to reach a given accuracy) of optimization algorithms applied to at least two systems: spin glasses and deep learning. Given an algorithm, the fluctuations of the halting time follow a universal distribution when the system is well tuned. This universality of the distribution is demonstrated by our computations: it is independent of input data and dimension. When the system is not well tuned this type of universality is destroyed. What makes this observation practically relevant is that the halting time fluctuations do not follow the universal distribution because either time is wasted for no gain in accuracy or the algorithm stops prematurely giving inaccurate results. This is consistent with the observations of Deift et al. (2014) in an analysis of the conjugate gradient algorithm.

1 INTRODUCTION

In this paper we discuss both the presence and application of universality in optimization algorithms with an emphasis on applications to deep learning. More precisely, we consider iterative algorithms (conjugate gradient for solving a linear system, gradient descent for spin glasses, and stochastic gradient descent for MNIST) to optimize an energy functional when the functional itself is random, the initial guess is random, or both. To each algorithm we attach a precise ϵ -dependent halting criteria for the algorithm and the number of iterations required, called the halting time, to meet this criteria is a random variable. Within each algorithm there is an intrinsic notion of dimension which we denote by N . The *halting time* $T_{\epsilon,N,\mathbb{A},E}$ depends on ϵ , N , the choice of algorithm \mathbb{A} , and the ensemble E (or probability distribution) put down on the functional and/or initial guess. We use the empirical distribution of $T_{\epsilon,N,\mathbb{A},E}$ to provide heuristics for understanding the qualitative performance of the algorithms.

The statement that “universality is present” in an algorithm is the observation that for sufficiently large N and $\epsilon = \epsilon(N)$, the halting time random variable satisfies

$$\tau_{\epsilon,N,\mathbb{A},E} := \frac{T_{\epsilon,N,\mathbb{A},E} - \mathbb{E}[T_{\epsilon,N,\mathbb{A},E}]}{\sqrt{\text{Var}(T_{\epsilon,N,\mathbb{A},E})}} \approx \tau_{\mathbb{A}}^*, \quad (1)$$

where $\tau_{\mathbb{A}}^*$ is a continuous random variable that depends only on the algorithm. The random variable $\tau_{\epsilon,N,\mathbb{A},E}$ is referred to as the *fluctuations* and when such an approximation appears to be valid we say that N and ϵ (and any other external parameters) are in the *scaling region*. Some remarks must be made:

- A statement like (1) is known to hold rigorously for some very simple algorithms but, in practice, it is verified experimentally. This was first done in Pfrang et al. (2014) and expanded in Deift et al. (2014).
- We only expect (1) to hold for a restricted class of ensembles E .
- $T_{\epsilon,N,\mathbb{A},E}$ is an integer-valued random variable and so a limit must be taken for it to become, after rescaling, a continuous distribution. This is the only reason N must be large — in practice, the approximation in (1) is seen for both small and large N .

1.1 THE DEMONSTRATION OF UNIVERSALITY

To give some historical context, we discuss the universality was first noticed in Pfrang et al. (2014) during the solution of the eigenvalue problem with the classical QR algorithm. Here the fundamental object is the QR factorization $(Q, R) = \text{QR}(A)$ where $A = QR$, Q is orthogonal (or unitary) and R is upper-triangular with positive diagonal entries. The QR algorithm applied to a Hermitian matrix A is given by the iteration

$$\begin{aligned} A_0 &:= A, \\ (Q_j, R_j) &:= \text{QR}(A_j), \\ A_{j+1} &:= R_j Q_j. \end{aligned}$$

Generically, $A_j \rightarrow D$ as $j \rightarrow \infty$ where D is a diagonal matrix whose diagonal entries are the eigenvalues of A . The halting time in Pfrang et al. (2014) was set to be the time of first deflation:

$$T_{\epsilon, N, \mathbb{A}, E}(A) = \min\{j : \sqrt{N(N-k)} \|A_j(k : N, 1 : k)\|_\infty < \epsilon \text{ for some } 1 \leq k \leq N-1\}.$$

Here $\|A\|_\infty$ refers to the maximum entry of a matrix A in absolute value and the notation $A(i : j, k : l)$ refers to the submatrix of A consisting of entries only in rows $i, i+1, \dots, j$ and in columns $k, k+1, \dots, l$. Thus the halting time for the QR algorithm is the time at which at least one off-diagonal block is appropriately small. Next, we have to discuss choices for the randomness, or ensemble E , by choosing different distributions on the entries of A . Four such choices for ensembles are:¹

- BE A is real-symmetric with iid Bernoulli ± 1 entries on and below the diagonal.
- GOE A is real-symmetric with iid standard normal entries below the diagonal. The entries on the diagonal are iid normal with mean zero and variance two.
- GUE A is complex-Hermitian with iid standard complex normal entries below the diagonal. The entries on the diagonal are iid complex normal mean zero and with variance two.
- QUE A is complex-Hermitian with probability density $\propto e^{-\text{tr}A^4} dA$. See Deift (2000) for details on such an ensemble and Olver et al. (2015) for a method to sample such a matrix. Importantly, the entries of the matrix below the diagonal are correlated.

Here we have continuous and discrete, real and complex, and independent and dependent ensembles but nevertheless we see universality in Figure 1 where we take $N = 150$ and $\epsilon = 10^{-10}$.

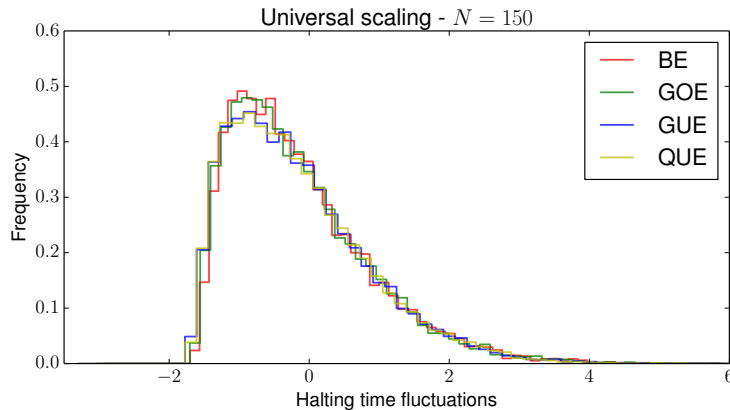


Figure 1: Empirical histograms for the halting time fluctuations $\tau_{\epsilon, N, \text{QR}, E}$ when $N = 150$, $\epsilon = 10^{-10}$ for various choices of ensembles E . This figure shows four normalized histograms, one each for $E = \text{BE}, \text{GOE}, \text{GUE}$ and QUE . It is clear that the fluctuations follow a universal law.

¹BE: Bernoulli ensemble; GOE: Gaussian orthogonal ensemble; GUE: Gaussian unitary ensemble; QUE: Quartic unitary ensemble

1.2 SPIN GLASSES AND DEEP LEARNING

A natural class of random fields is the class of Gaussian random functions on a high dimensional sphere, known as p -spin spherical spin glass models in the physics literature (in the Gaussian process literature they are known as isotropic models). From an optimization point of view, minimizing the spin glass model’s Hamiltonian has become a showcase for a central question in deep learning: Do local minima and saddle points, due to the non-convex nature of landscapes, present an obstacle in the training of a system? For a deep learning application we use the MNIST database discussed further in Section 4.

Dauphin et al. (2014) observes that saddle points can be an issue in optimization. In contrast Sagun et al. (2015) and the experimental second section of Choromanska et al. (2014) jointly argue that saddle points do not present a serious obstacle, and add that any local minima found should be sufficient for applications. However, Sagun et al. (2015) and Choromanska et al. (2014) hold different perspectives on what the qualitative similarities between optimization in spin glasses and deep learning might imply. The latter asserts a direct connection between the two systems based on these similarities. On the contrary, the former argues that these similarities hint at universal behaviors that are generically observed in vastly different systems rather than emphasizing a direct connection.

One of the main motivators for the comparison of spin glasses and deep learning is due to the amount of knowledge we have on the Gaussian spherical spin glass function. Auffinger et al. (2012) gives asymptotic bounds on the value of the ground state as well as the exponential behavior of the mean number of critical points below a given energy level. In particular, it is shown that when the dimension is large, the bulk of the local minima tend to have the same value which is slightly above the ground state. We call this level the *floor* level of the function, meaning that an algorithm can reach it within a reasonable amount of time, even though we know there are critical points at the lower energies. The simulations of the floor in spin glass, and experimental observation of floor in an MNIST set up can be found in Sagun et al. (2015) showing the universal connection.

1.2.1 SETUP AND FIRST OBSERVATIONS

- Given data (i.e., from MNIST) and a measure $L(x^\ell, w)$ for determining the cost that is parametrized by $w \in \mathbb{R}^N$, the training procedure aims to find a point w^* that minimizes the empirical training cost while keeping the test cost low. We use x^ℓ for $\ell = 1, \dots, S$ where S is as large as the data that is available to denote the training samples. The total training cost is given by

$$\mathcal{L}_{\text{Train}}(w) = \frac{1}{S} \sum_{\ell=1}^S L(x^\ell, w). \quad (2)$$

Note that the number of terms in the sum does not depend on the dimension N of the system.

- The Hamiltonian (or energy) of the simplest complex² spherical spin glass model is given by:

$$H_N(w) = \frac{1}{N} \sum_{i,j,k} x_{ijk} w_i w_j w_k. \quad (3)$$

The couplings $x_{(\cdot)} \sim \text{Gaussian}(0, 1)$ represent the strength of forces between triplets of spins. The state of the system is represented by $w \in S^{N-1}(\sqrt{N}) \subset \mathbb{R}^N$. The spin glass system tends to find a configuration w that has a low energy.

Some of the apparent differences are the following: At a fixed point w , when there is a lot of samples, the law of large numbers kicks in, and the function $\mathcal{L}_{\text{Train}}(w)$ converges to $\int L(x, w) dP(x)$ where P is the unknown distribution from which the examples are sampled. But $H_N(w)$ is a Gaussian random variable with mean zero and variance N (because of this, the local minima of (3) are typically found at values around a negative constant multiple of N). The domain of the Hamiltonian is a compact

²2-spin spherical spin glass, sum of $x_{ij} w_i w_j$ terms, has exactly $2N$ critical points. When $p \geq 3$, p -spin model has exponentially many critical points with respect to N . For the latter case, complexity is a measure on the number of critical points in an exponential scale. Deep learning problems are suspected to be complex in this sense.

space and the couplings are independent Gaussian random variables whereas the inputs for (2) are very dependent and the functional has a non-compact domain. Also, (2) is non-negative and its interesting values are when the explorer is on the inverse image of $[0, \epsilon]$, whereas p -spin is a mean zero field and is interesting near its *floor* value whose typical size is at the order of N .

1.3 SUMMARY OF RESULTS

We discuss the presence of universality in algorithms that are of a very different character. The conjugate gradient algorithm, discussed in Section 2, effectively solves a convex optimization problem. Gradient descent and stochastic gradient descent applied in the spin glass setting (discussed in Section 3) and in context of deep learning (MNIST, discussed in Section 4) is a much more complicated non-convex optimization process. Despite the fact that these algorithms share very little geometry in common, we demonstrate three things they share:

- A scaling region in which universality appears and performance is good.
- Cases existing outside the scaling region where the computation is either ineffective or inefficient. Performance is lost.
- A moment-based indicator for the scaling region (where performance is good).

2 THE CONJUGATE GRADIENT ALGORITHM

The conjugate gradient algorithm (Hestenes & Steifel, 1952) for solving the $N \times N$ linear system $Ax = b$ when $A = A^*$ is positive definite is an iterative procedure to find the minimum of the convex quadratic form:

$$y^*Ay - y^*b,$$

where $*$ denotes the conjugate-transpose operation. Given an initial guess x_0 (we use $x_0 = b$), compute $r_0 = b - Ax_0$ and set $p_0 = r_0$. For $k = 1, \dots, N$,

1. Compute $r_k = r_{k-1} - a_{k-1}Ap_{k-1}$ where³ $a_{k-1} = \langle r_{k-1}, r_{k-1} \rangle / \langle p_{k-1}, Ap_{k-1} \rangle$.
2. Compute $p_k = r_k + b_{k-1}p_{k-1}$ where $b_{k-1} = \langle r_k, r_k \rangle / \langle r_{k-1}, r_{k-1} \rangle$.
3. Compute $x_k = x_{k-1} + a_{k-1}p_{k-1}$.

If A is strictly positive definite $x_k \rightarrow x = A^{-1}b$ as $k \rightarrow \infty$. Geometrically, the iterates x_k are the best approximations of x over larger and larger affine Krylov subspaces \mathcal{K}_k ,

$$\|Ax_k - b\|_A = \min_{x \in \mathcal{K}_k} \|Ax - b\|_A, \\ \mathcal{K}_k = x_0 + \text{span}\{r_0, Ar_0, \dots, A^{k-1}r_0\}, \quad \|x\|_A^2 = \langle x, A^{-1}x \rangle,$$

as $k \uparrow N$. The quantity one monitors over the course of the conjugate gradient algorithm is the norm $\|r_k\|$:

$$T_{\epsilon, N, CG, E}(A, b) := \min\{k : \|r_k\| < \epsilon\}.$$

In exact arithmetic, the method takes at most N steps: In calculations with finite-precision arithmetic the number of steps can be much larger than N and the behavior of the algorithm in finite-precision arithmetic has been the focus of much research (Greenbaum, 1989; Greenbaum & Strakos, 1992). What is important for us here is that it may happen that $\|r_k\| < \epsilon$ but the true residual $\hat{r}_k := b - Ax_k$ (which typically differs from r_k in finite-precision computations) satisfies $\|\hat{r}_k\| > \epsilon$.

2.1 UNIVERSALITY

Now, we discuss our choices for ensembles E of random data. In all computations, we take $b = (b_j)_{1 \leq j \leq N}$ where each b_j is iid uniform on $(-1, 1)$. We construct positive definite matrices A by $A = XX^*$ where $X = (X_{ij})_{1 \leq i \leq N, 1 \leq j \leq M}$ and each $X_{ij} \sim \mathcal{D}$ is iid for some distribution \mathcal{D} . We make the following three choices for \mathcal{D} :⁴

³We use the notation $\|y\|^2 = \langle y, y \rangle = \sum_j |y_j|^2$ for $y = (y_1, y_2, \dots, y_N) \in \mathbb{C}^N$.

⁴PDE: Positive definite Bernoulli ensemble; LOE: Laguerre orthogonal ensemble; LUE: Laguerre unitary ensemble

PBE \mathcal{D} a Bernoulli ± 1 random variable (equal probability).

LOE \mathcal{D} is a standard normal random variable.

LUE \mathcal{D} is a standard complex normal random variable.

In Deift et al. (2014) and Deift et al. (2015) it was demonstrated that universality is present when $M = N + \lfloor cN \rfloor$ and ϵ is small, but fixed. Universality is not present when $M = N$ and this can be explained by examining the distribution of the condition number of the matrix A in the LUE setting (Deift et al., 2015). We demonstrate this again in Figure 2(a). We also demonstrate that universality does indeed fail for $M = N$ in Figure 2(b).

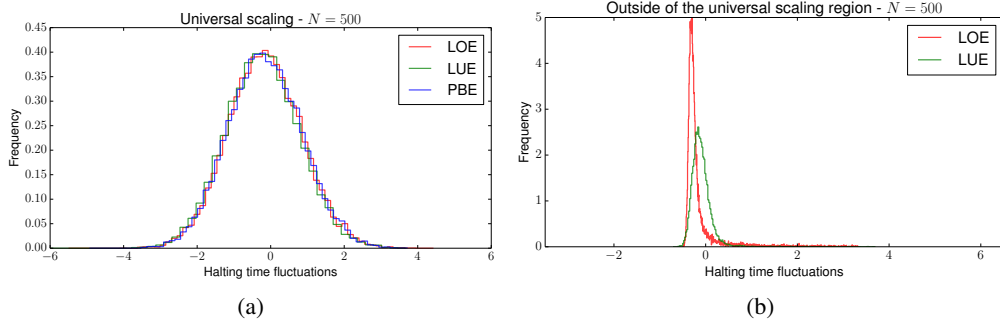


Figure 2: Empirical histograms for the halting time fluctuations $\tau_{\epsilon, N, CG, E}$ when $N = 500$, $\epsilon = 10^{-10}$ for various choices of ensembles E . (a) The scaling $M = N + 2\lfloor N \rfloor$ demonstrating the presence of universality. This plot shows three histograms, one each for $E = \text{LUE}, \text{LOE}$ and PBE . (b) The scaling $M = N$ showing two histograms for $E = \text{LUE}$ and LOE and demonstrating the non-existence of universality.

2.2 EFFICIENCY VERSUS ACCURACY

One way to understand the breakdown of universality in the $M = N$ case is to examine the efficiency versus accuracy trade-off for the algorithm. We fix $N = 500$, $M = N$ and vary ϵ in the LOE case. Our measure of accuracy is $\|\hat{r}_k\|$ which vanishes in the case of perfect accuracy and the measure of efficiency is the halting time. In Figure 3 we plot ensemble averages of efficiency versus accuracy for $\epsilon = 10^{-j}$, $j = 1, 2, \dots$. A sharp plateau in the accuracy is seen, indicating that the extra computation for small values of ϵ is unnecessary. In this example and the spin glass example below, the extra computation without a gain in accuracy indicates the loss of universality.

3 SPIN GLASSES AND GRADIENT DESCENT

The gradient descent algorithm for the Hamiltonian of the p -spin spherical glass will find a local minimum of the non-convex function (3). Since variance of $H_N(w)$ is typically of order N , a local minimum has size N . More precisely, by Auffinger et al. (2012), the energy of the floor level where most of local minima are located is asymptotically at $-2\sqrt{2/3}N \approx -1.633N$ and the ground state is around $-1.657N$. A randomly chosen point on the sphere has energy near \sqrt{N} . The algorithm starts by picking a random element w of the sphere $S^{N-1}(\sqrt{N})$ as a starting point for each trial. For a fixed dimension N , accuracy ϵ , and an environment sampled by an ensemble E ,

1. Calculate the gradient steps: $w^{t+1} = w^t - \eta_t \nabla_w H(w^t)$
2. Normalize the gradient vector to the sphere: $\sqrt{N} \frac{w^{t+1}}{\|w^{t+1}\|} \leftarrow w^{t+1}$
3. Stop when the norm of the gradient size is below ϵ and record $T_{\epsilon, N, GD, E}$

We vary the environment for each trial and introduce ensembles by setting $x_{(\cdot)} \sim \mathcal{D}$ for a number of choices of distribution \mathcal{D} .

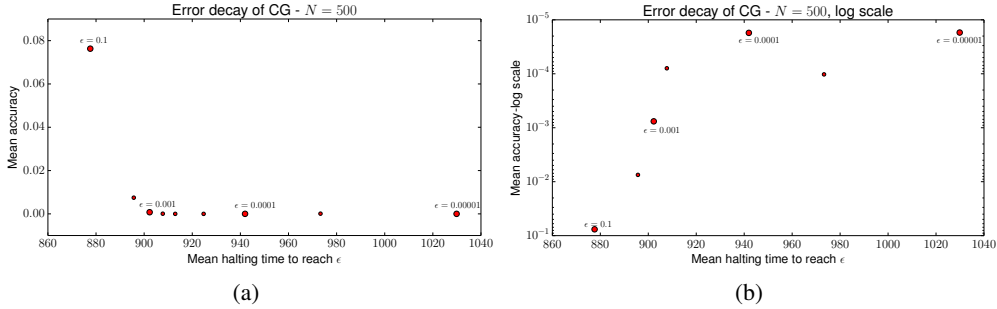


Figure 3: When $M = N = 500$ we plot the sample average of the halting time versus the sample average of the accuracy for various choices of ϵ . Accuracy is measured as $\|\hat{r}_k\|$ when the algorithm is halted — a smaller error value indicates better results. It is clear that the accuracy breaks down at around $\epsilon = 10^{-6}$ in the sense that increasing ϵ increases the computation time but does not increase the accuracy. This type of behavior appears to be a hallmark of universality breakdown. This particular breakdown is caused by round-off error.

Since the algorithm is attracted to a local minimum where the norm of the gradient is zero, it seems natural to put a constraint on the norm of the gradient. In our experiments, we get the same universal distributions for other criteria such as bounding the successive energy difference. One can also find a way to implement stochastic gradient descent on spin glasses by creating the field as a sum of smaller fields. Interestingly, it gives the same statistics and is smaller depending on how many smaller fields used. For further details see Sagun et al. (2015).

3.1 UNIVERSALITY

The above procedure is repeated 10,000 times for different ensembles (choices for \mathcal{D}), and for different accuracies when the ensemble is fixed. In each case we exhibit the universal halting time presenting evidence that $\tau_{\epsilon, N, \text{GD}, E}$ is independent of the ensemble and accuracy within a range of hyperparameters, see Figure 4.

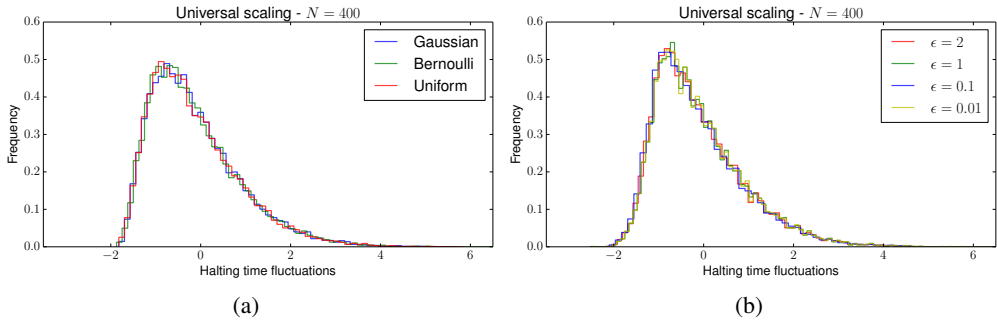


Figure 4: Universality across distributions: We choose $\mathcal{D} \sim \text{Gaussian}(0, 1)$, \mathcal{D} uniform on $(-(3/2)^{1/3}, (3/2)^{1/3})$ and \mathcal{D} Bernoulli $\pm 1/\sqrt{2}$ with equal probability. (a) $N = 400$, the step size is 0.2 and $\epsilon = 0.3$. (b) The same information but letting ϵ vary in $[0.01, 2]$. The halting time fluctuations follow a universal law.

One can push the statistics out of the scaling region by tweaking the step size. Decreasing the step size will scale the mean halting time proportionately, however the standard deviation grows faster which results in degenerate distributions. This observation is demonstrated for a small, fixed step size for two different dimensions in Figure 5.

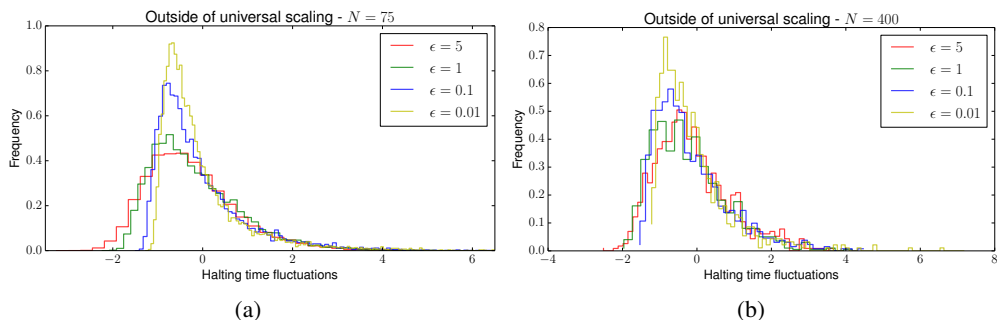


Figure 5: These histograms demonstrate the loss of universality when the step size is 0.05, for $D \sim \text{Gaussian}(0, 1)$. (a) $N = 75$. (b) $N = 400$.

On the other extreme, a very large step size will never converge. The message here is that one should increase the step size as much as one can when there is decay in the energy. Once there is no progress, try the largest, yet smaller, value that gives rise to decay in energy. Note that this is common practice among many deep learning practitioners.

3.2 ACCURACY AND EFFICIENCY

In the spin glass setting, the floor value gives a natural bound on the value that the Hamiltonian can practically reach. That value is above the ground state at an energy level where most local minima lie. This level presents a natural barrier for an algorithm like the gradient descent. Our method will locate a local minimum near the floor level quite fast, and the difference in energy between the ground state and the points gradient descent locates is negligible. Therefore a natural measure of performance at the point w^* would be by looking at $H(w^*)/(\text{floor value})$. Increasing the dimension means the local minima are moving closer to the floor value. So, for a fixed accuracy we expect get better results in higher dimensions. Moreover, we have a similar accuracy vs. efficiency trade-off as observed in the conjugate gradient algorithm, see Figure 6.

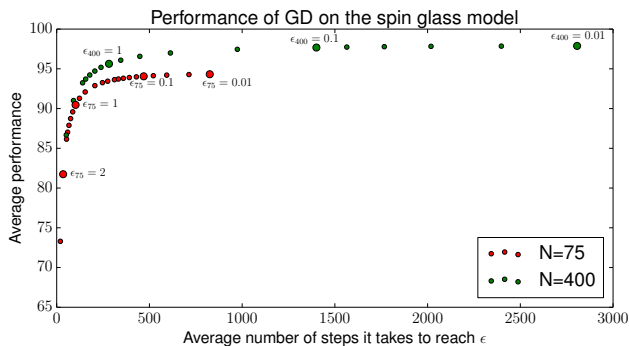


Figure 6: When $N = 75$ and $N = 400$ we plot the sample average of the halting time versus the performance for various choices of ϵ . Performance is measured by how close the energies get to the asymptotic limit value at the floor. Note that this value is larger, but not by considerable amount, than the ground state. Larger accuracy values indicates better results. It is clear that the beyond an accuracy level of 0.7 for $N = 75$, and 1.0 for $N = 400$, increasing computation time does not result in significance performance gain.

4 MNIST

MNIST dataset consists of 60,000 samples of training examples and 10,000 samples of test examples. A first attempt would be to construct a two layer fully connected network with rectified linear activation units, and a cross entropy cost attached at the end. The model is trained by the stochastic gradient descent algorithm which locates a small value of $\mathcal{L}_{\text{Train}}(w)$.

The training set can be treated as the ensemble and at each trial one can randomly sample a subset from the training-ensemble. In order to obtain a large number of samples, at each trial we sample 100 examples to form the cost function examples, and train a small, one-hidden layer network with 50 hidden units. The mini-batch size is chosen to be 100, in other words we perform gradient descent on the cost surface with $S = 100$. As a result we get rid of unwanted noise in the mini-batch gradients, which ensures that the stopping criteria is precise, and there is no additional noise present. Recall, that the intended randomness comes from sampling small training sets from the larger training set, and picking random initial points on the landscape. Two natural stopping criteria are constraints on the norm of the gradient, and successive difference in cost decrease. We demonstrate universal fluctuations in the halting time in Figure 7. We emphasize that due to the data driven nature of this method, the histograms should not be expected to be as well-resolved as in the case of the spin glass model or conjugate gradient. Additionally, since we, in essence, have only one ensemble at our disposal (the MNIST dataset) we use insensitivity to the choice of ϵ as our indicator for universality.

As a comparison we take the same setup and set the mini-batch size to 1 and repeat the experiment with stochastic gradient descent (SGD). We refer the reader to Sagun et al. (2015) for a discussion of this method. The stopping criteria for SGD is when the average of the differences of the last 5 mini-batch costs is below a given accuracy. In the universality scaling regime, even with the additional noise from SGD, we find the same halting time distribution across various accuracy levels.

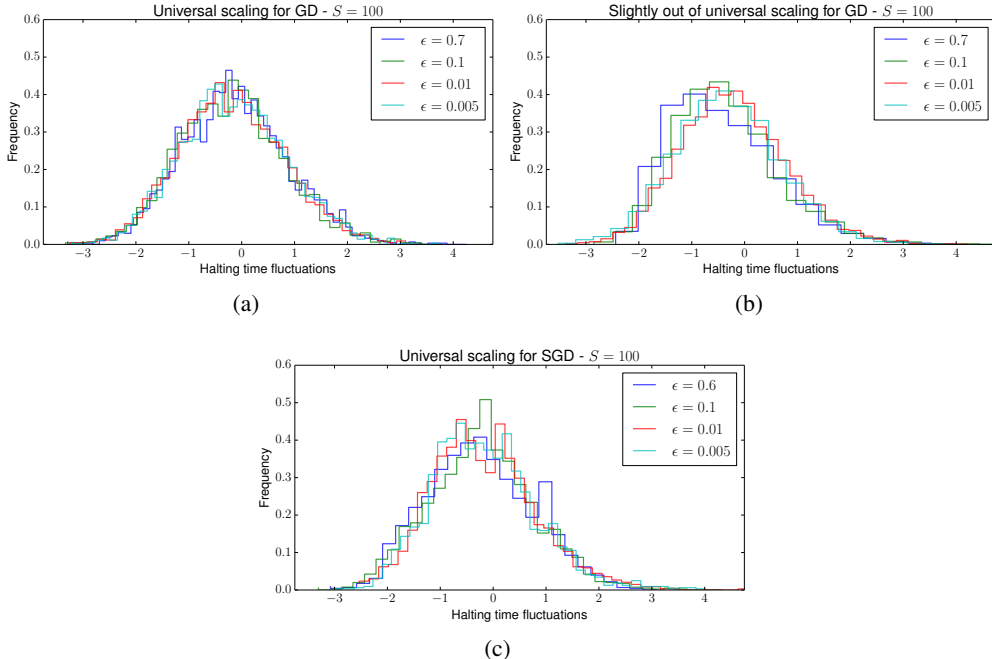


Figure 7: A demonstration of universality in MNIST. The halting time fluctuations are relatively insensitive to the choice of ϵ . (a) A universal regime with step size = 0.02, gradient descent stops when the cost on training set is below ϵ . (b) A non-universal regime with the same setup but step size = 0.2. The histograms shift to become more symmetrical as accuracy tightens. (c) Again, the same setup when step size is = 0.02, but using SGD with mini-batch size 1. While additional noise is introduced by using SGD, this appears to be a universal regime.

Recall that each model has two layers of randomness: the ensemble, and the random initial point. In a deep learning setting a trivial observation is that the initial cost is almost the same no matter what initial random point one chooses, which is not the case in spin glass as noted earlier. This essentially leaves us with only a single layer of randomness assuming we perform gradient descent. However, in practice, one never does gradient descent, and the stochastic gradient descent puts that extra layer of randomness to the system.

4.1 ACCURACY

For each trial sample 100 examples from the test set and count how many of them are correctly classified by the classifier. Such a tiny network still manages to get well above random guessing. The point here is that there is a region in which we expect to see the universal halting time distribution and before that level we can't get full performance from our model, after that level we are just pushing too much for no decent return.

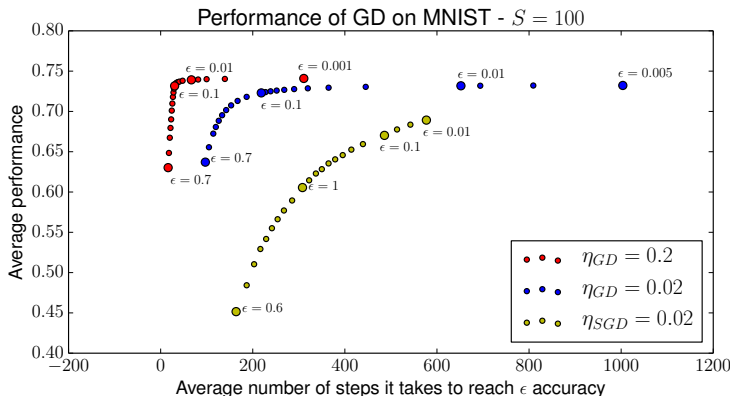


Figure 8: Gradient descent on MNIST with only 100 examples in the training set. On the left step size is 0.02, on the right it is 0.2. We observe the same accuracy vs efficiency trade-off that is observed in the other algorithms.

5 A NORMALIZED-MOMENTS ANALYSIS TO DETERMINE THE OPTIMAL REGIME

To quantify if, for a certain value of the parameters, one is in the scaling region (which we associate to a region of optimal performance) we use the normalized third and fourth moments of the data, also referred to as the skewness and kurtosis.

Universality heuristic: *For a quantitative test of universality, we say certain parameters values are in the scaling region if the relative difference of any two computed skewness (resp. kurtosis) values compared across ensembles is small.*

This principle is left vague on purpose but it intuitively holds in the $M = N + 2\lfloor\sqrt{N}\rfloor$ case but not for the $M = N$ case as Figure 9 shows.

In preparation for the MNIST setting where only one ensemble is present and we cannot directly apply the universality heuristic, we analyze the moments of the halting time distribution across both ensembles as in Figure 9 and as ϵ varies for a fixed ensemble. In this spin glass setting as accuracy increases the skewness and kurtosis also increase as one leaves the scaling region. See Figure 10(a) for a case where the universality heuristic clearly applies. Then, Figure 10(b) indicates universality for $\eta = 0.2$ and $0.01 \leq \epsilon \leq 0.7$ if we apply the universality heuristic despite the fact we are not comparing across ensembles.

For our MNIST experiments due to the increasing cost of computing we restricted ourselves for $\eta_{GD} = 0.2$ and $\eta_{GD} = 0.02$. Therefore the case of slightly-out-of-universal regime does not

$M = N$	Skewness	Kurtosis	$M = N + 2\lfloor\sqrt{N}\rfloor$	Skewness	Kurtosis
LUE	15.7	288.5	LUE	0.07	3.0
LOE	5.1	35.2	LOE	0.08	3.1
PBE	5.9	69.3	PBE	0.08	3.0

Figure 9: For the cases $M = N + 2\lfloor\sqrt{N}\rfloor$ and $M = N$, $N = 500$, $\epsilon = 10^{-8}$ with the averages taken over 16,000 samples, we tabulate the skewness and kurtosis of the empirical halting time. In the $M = N + 2\lfloor\sqrt{N}\rfloor$ (right) it is clear that these normalized moments nearly coincide and they are quite distinct for $M = N$ (left).

$\eta = 0.2$	Skewness	Kurtosis
Gaussian	1.10	4.58
Bernoulli	1.10	4.56
Uniform	1.10	4.54

(a)

Gaussian $\eta = 0.05$	Skewness	Kurtosis	Gaussian $\eta = 0.2$	Skewness	Kurtosis
$\epsilon = 0.7$	0.82	3.73	$\epsilon = 0.7$	0.5	2.56
$\epsilon = 0.1$	0.98	4.26	$\epsilon = 0.1$	0.76	3.60
$\epsilon = 0.01$	1.38	5.25	$\epsilon = 0.01$	0.83	3.62
$\epsilon = 0.005$	2.41	12.30	$\epsilon = 0.005$	1.40	5.66

(b)

Figure 10: (a) In the universality scaling region across different distributions with averages over 10,000 samples. The moments clearly satisfy our universality heuristic. (b) In the Gaussian case for the step size $\eta = 0.05$, $N = 75$, $\eta = 0.05$, $N = 400$ with the averages taken over 10,000 samples the normalized moments nearly are distinct. But in the universal regime for $\eta = 0.02$ the normalized moments are much less sensitive to ϵ .

demonstrate a striking difference one might have had if she picked the wrong hyper-parameters. Even then the skewness and kurtosis is more consistent in the universal regime, see Figure 11.

$\eta_{GD} = 0.2$	Skewness	Kurtosis	$\eta_{GD} = 0.02$	Skewness	Kurtosis
$\epsilon = 0.7$	0.65	3.3	$\epsilon = 0.7$	0.24	3.20
$\epsilon = 0.1$	0.74	4.22	$\epsilon = 0.1$	0.24	3.21
$\epsilon = 0.01$	0.3	3.3	$\epsilon = 0.01$	0.21	3.06
$\epsilon = 0.005$	0.16	3.2	$\epsilon = 0.005$	0.17	3.00

Figure 11: For the cases of step sizes $\eta_{GD} = 0.2$ and $\eta_{GD} = 0.02$, $S = 100$, with the averages taken over 5,000 samples, we tabulate the skewness and kurtosis of the empirical halting time. In the $\eta_{GD} = 0.02$ (right) it is clear that these normalized moments nearly coincide and they are not as similar for $\eta_{GD} = 0.2$ (left). If we apply the universality heuristic here, despite not having multiple ensembles, we would claim universality for $\eta_{GD} = 0.02$. It is evident that by pushing the step size further one can get more drastic differences for the skewness and kurtosis, albeit with the greater cost of additional computation time.

6 CONCLUSIONS AND FUTURE WORK

What constitutes a good set of hyper-parameters for a given algorithm? How can we go beyond inspection when tuning a system? We believe this research attempts to answer these questions in a robust way and quantitative way. Future work will be along the lines of using these heuristics, and improving them, to guide both algorithm development and algorithm tuning.

We also believe that this work further validates the broad claims made in Deift et al. (2015) that universality is present in all or nearly all (sensible) computation. As a final demonstration of this

idea we, jointly with our previous collaborator Uğur Güney⁵, perform a Google™ search query experiment. A set of random words (an ensemble) is provided and the system chooses each word as a search query. The result given by Google™ indicates the search time and this is taken as the halting time. This is a black box example of decision making and we compare our results with the theoretical prediction for an experiment performed on human decision making Bakhtin & Correll (2012). The mean duration is 0.45s with standard deviation 0.11s, and the fluctuations seem to follow the distribution found in Bakhtin & Correll (2012) (see the solid curve in Figure 12), the skewness is 2.82 and the kurtosis is 37. Future work will be in the direction of exploring this connection. It

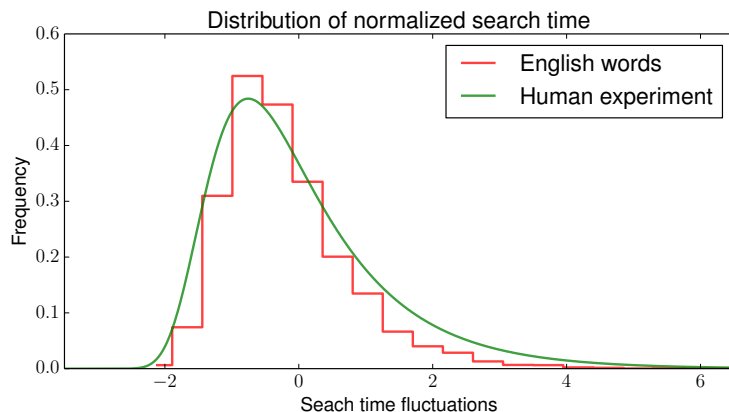


Figure 12: Word query time fluctuations over 6,000 samples compared with the theoretically predicted curve in Bakhtin & Correll (2012).

is evident that more observations have yet to be made in identifying the underlying principles of the algorithms that are increasingly part of our life.

ACKNOWLEDGMENTS

We thank Percy Deift for valuable discussions and Gérard Ben Arous for his mentorship throughout the process of this research. The first author thanks very much to Uğur Güney for his availability for support and valuable contributions in countless implementation issues. This work was partially supported by the National Science Foundation under grant number DMS-1303018 (TT).

REFERENCES

- Auffinger, Antonio, Arous, Gérard Ben, and Černý, Jiří. Random Matrices and Complexity of Spin Glasses. *Communications on Pure and Applied Mathematics*, 66(2):165–201, sep 2012. doi: 10.1002/cpa.21422.
- Bakhtin, Yuri and Correll, Joshua. A neural computation model for decision-making times. *Journal of Mathematical Psychology*, 56(5):333–340, oct 2012. doi: 10.1016/j.jmp.2012.05.005.
- Choromanska, Anna, Henaff, Mikael, Mathieu, Michael, Ben Arous, Gérard, and LeCun, Yann. The Loss Surface of Multilayer Networks. November 2014. URL <http://arxiv.org/abs/1412.0233v2>.
- Dauphin, Yann N, Pascanu, Razvan, Gulcehre, Caglar, Cho, Kyunghyun, Ganguli, Surya, and Bengio, Yoshua. Identifying and attacking the saddle point problem in high-dimensional non-convex optimization. In Ghahramani, Z, Welling, M, Cortes, C, Lawrence, N D, and Weinberger, K Q (eds.), *Advances in Neural Information Processing Systems 27*, pp. 2933–2941. Curran Associates, Inc., June 2014.
- Deift, Percy. *Orthogonal Polynomials and Random Matrices: a Riemann-Hilbert Approach*. Amer. Math. Soc., Providence, RI, 2000.

⁵The code is accessible at Uğur’s GitHub repository which can be accessed at Güney

- Deift, Percy, Menon, Govind, Olver, Sheehan, and Trogdon, Thomas. Universality in numerical computations with random data. *Proc. Natl. Acad. Sci. U. S. A.*, 111(42):14973–8, oct 2014. ISSN 1091-6490. doi: 10.1073/pnas.1413446111.
- Deift, Percy, Menon, Govind, and Trogdon, Thomas. On the condition number of the critically-scaled Laguerre Unitary Ensemble. *arXiv Prepr. arXiv1507.00750*, jul 2015.
- Greenbaum, Anne. Behavior of slightly perturbed Lanczos and conjugate-gradient recurrences. *Linear Algebra Appl.*, 113:7–63, 1989. ISSN 00243795. doi: 10.1016/0024-3795(89)90285-1.
- Greenbaum, Anne and Strakos, Zdenek. Predicting the Behavior of Finite Precision Lanczos and Conjugate Gradient Computations. *SIAM J. Matrix Anal. Appl.*, 13(1):121–137, jan 1992. ISSN 0895-4798. doi: 10.1137/0613011.
- Güney, V Uğur. Decision time universality. URL <https://github.com/vug/decision-time-universality>.
- Hestenes, Magnus and Steifel, Eduard. Method of Conjugate Gradients for solving Linear Systems. *J. Res.*, 20:409–436, 1952.
- Olver, Sheehan, Rao, N Raj, and Trogdon, Thomas. Sampling unitary ensembles. *Random Matrices Theory Appl.*, 4(1):1550002, 2015. ISSN 2010-3263. doi: 10.1142/S2010326315500021.
- Pfrang, Christian W, Deift, Percy, and Menon, Govind. How long does it take to compute the eigenvalues of a random symmetric matrix? *Random matrix theory, Interact. Part. Syst. Integr. Syst. MSRI Publ.*, 65:411–442, 2014.
- Sagun, Levent, Güney, V. Uğur, Arous, Gérard Ben, and LeCun, Yann. Explorations on high dimensional landscapes. 2015. workshop contribution at ICLR 2015.